Author's Accepted Manuscript

Many particle magnetic dipole-dipole and hydrodynamic interactions in magnetizable stent assisted magnetic drug targeting

P.J. Cregg, Kieran Murphy, Adil Mardinoglu, Adriele Prina-Mello

www.elsevier.com/locate/jmmm

Cite this article as: P.J. Cregg, Kieran Murphy, Adil Mardinoglu and Adriele Prina-Mello, Many particle magnetic dipole-dipole and hydrodynamic interactions in magnetizable stent assisted magnetic drug targeting, *Journal of Magnetism and Magnetic Materials*, doi:10.1016/j.jmmm.2010.01.038

This is a PDF file of an unedited manuscript that has been accepted for publication. As a service to our customers we are providing this early version of the manuscript. The manuscript will undergo copyediting, typesetting, and review of the resulting galley proof before it is published in its final citable form. Please note that during the production process errors may be discovered which could affect the content, and all legal disclaimers that apply to the journal pertain.

Many particle magnetic dipole-dipole and hydrodynamic interactions in magnetizable stent assisted magnetic drug targeting

P.J. Cregg[a,*], Kieran Murphy[a], Adil Mardinoglu[a], Adriele Prina-Mello[b,*]

[a]*SEAM Centre, Materials Characterisation and Processing Group, Waterford Institute of Technology, Waterford, Ireland*
[b]*CRANN and School of Physics, Trinity College, Dublin 2, Ireland*

Abstract

The implant assisted magnetic targeted drug delivery system of Avilés, Ebner and Ritter is considered both experimentally (*in vitro*) and theoretically. The results of a 2D mathematical model are compared with 3D experimental results for a magnetizable wire stent. In this experiment a ferromagnetic, coiled wire stent is implanted to aid collection of particles which consist of single domain magnetic nanoparticles (radius ≈ 10 nm). In order to model the agglomeration of particles known to occur in this system, the magnetic dipole-dipole and hydrodynamic interactions for multiple particles are included. Simulations based on this mathematical model were performed using open source C++ code. Different initial positions are considered and the system performance is assessed in terms of collection efficiency. The results of this model show closer agreement with the measured *in vitro* experimental results and with the literature. The implications in nanotechnology and nanomedicine are based on the prediction of the particle efficiency, in conjunction with the magnetizable stent, for targeted drug delivery.

Keywords: magnetic drug targeting, high gradient magnetic separation (HGMS), magnetic nanoparticles, simulation, dipole-dipole interaction, hydrodynamic interaction, magnetizable stent.

---

*Corresponding authors
Email addresses:* `pjcregg@wit.ie` (P.J. Cregg), `prinamea@tcd.ie` (Adriele Prina-Mello)

1. Introduction

The development of more effective drug treatment methodologies is an area of much research. In most drug delivery systems much of any drug administered to patients does not reach its target site. The aim of the drug targeting is to decrease the amount of drug delivered to healthy tissue, while maintaining the therapeutic action at the desired site. One such approach is magnetic drug targeting (MDT). For instance magnetic particles can be employed as carriers in a cancer treatment, thereby avoiding the side effects of conventional chemotherapy [1, 2]. MDT typically uses an external magnetic field source to capture and retain magnetic drug carrier particles (MDCPs) at a specific site after being injected into the body. Studies have shown that MDT is a relatively safe and effective methodology for targeting drugs to a specific site in the body [3, 4, 5]. However, there are some significant limitations of MDT. One limitation associated with MDT is the gradient problem, that is the magnetic force requires a magnetic field gradient. Specifically it can be difficult using external magnets only to target areas deep within the body, without targeting the surface more strongly [6]. To overcome this problem several authors [7, 8, 9, 10, 11, 12, 13, 14, 15, 16] have proposed implanting ferromagnetic materials such as wires, seeds and stents within the body. Of the various IA-MTD implants suggested by Ebner, Ritter and co-workers [9, 10, 11, 12, 13, 14, 15, 16], we consider a magnetizable stent as the implant, with MDCPs containing magnetic single domain nanoparticles. Previously, by considering high gradient magnetic separation, Mikkelsen *et al.* [17] have included both the hydrodynamic and dipole-dipole interactions for the case of low magnetic fields. Also, Mehasni *et al.* have considered the effect of magnetic dipole-dipole interaction on the performance of high gradient magnetic separation systems [18]. Some of the present authors have previously considered the effect of the interactions for two MDCPs on the agglomeration of the

2

MDCPs [19]. Here, we calculate the effect of interactions of many particles on the collection efficiency of the system leading to the agglomeration of particles. Avilés *et al.* [14] compared the (non interacting) particle model of this stent system with *in vitro* experimental arrangement using a ferromagnetic stent made in the shape of a coil. Their results indicated that at low fluid velocity more particles were collected than predicted. Furthermore, they suggested that particle agglomeration (due to interparticle interactions) might explain this. With this in mind, we have further developed their mathematical model to include both dipole-dipole and hydrodynamic interactions between many MDCPs. These theoretical results are presented here and are compared with the experimental results of Avilés *et al.* [14] and new *in vitro* experiments. Simulations are performed using OpenFOAM a finite volume simulation C++ library.

2. Experimental Setup

In this experiment ferromagnetic particles with diameter of $0.86\,\mu$m containing 45.8 wt% magnetite are used as the MDCPs (Polysciences Europe GmbH). Stainless steel (SS) 430 (California Fine Wire Co.) is taken as the wire material for the stent with a $62.5\,\mu$m radius following Avilés *et al.* [14]. The stent is prepared by looping a length of wire, L, into a 2 cm long coil having a 0.04 cm radius containing 10 loops, N_l, with 0.2 cm between each loop. Between use, each stent wire is cleaned by a 30 minute sonication in ethanol. A set of 15 identical coil stents are made and cleaned for the full MDT experimental testing.

The stent is firmly positioned within a borosilicate glass capillary tube by interference adhesion against the inner surface of the tube (radius of 0.04 cm). Controlled thickness capillary tubing is used to maximize the contrast between stent and glass curvature for real time video imaging and particle detection. Furthermore, this is also eliminates any turbulence caused by the irregular glass surface roughness. In this experiment we use a capillary glass tube (0.04 cm radius) and particle size proportionally similar to Avilés *et al.* [14].

The experimental setup is shown in Figure 1. It consists of a capillary glass
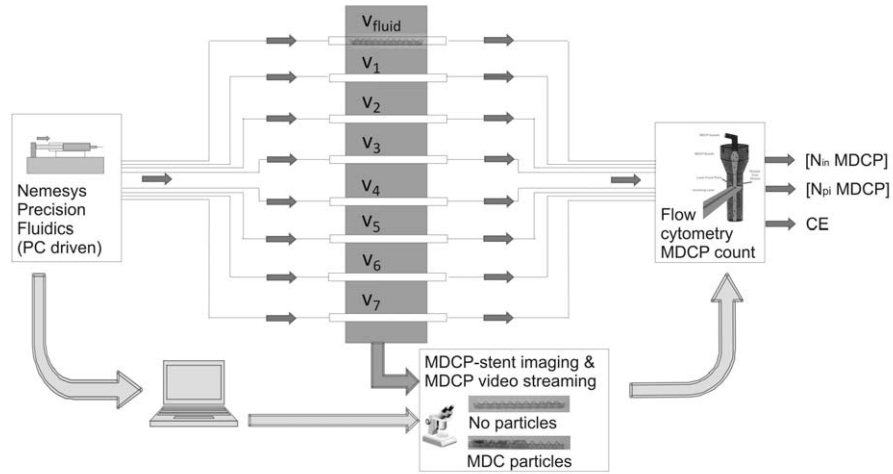
3

Figure 1: Schematic diagram of the *in vitro* experimental setup used to study a stent-based IA-MDT system.

tube with a regularly spaced coil stent, an equally spaced pair of single NdFeB permanent magnets (in opposition), connected by tygon tubing to a 2.5 ml syringe where one end is connected to a high precision syringe pump to supply the suspension of MDCPs and the other end is connected to a collection system for collection efficiency measurements. The setup also comprises an inverted microscope connected to a CCD camera for high resolution imaging (QI Micropublisher, USA) and video acquisition. Magnetic field strength is measured by a Hall probe gaussmeter (Lake Shore, USA). The particle, pre- and post-wash buffer solution where precisely injected by using 2.5 ml syringes connected to a high precision syringe pump system and software where it is possible to control injection direction, volume injected, flow rate in relation to the fluid solution injected (Nemesys system, Cetoni Gmbh, Germany). For each solution injected the total concentration is measured, pre- and post- experiment, by flow cytometry technique (Accuri, C6 Flow Cytometer and CFlow plus software, UK). Thus, each experiment had the same initial volume of solution.

Microscopy imaging is carried out using an Olympus microscope (Olympus,

4

Japan) connected to a QI micropublisher camera driven by ImagePro software (Media Cybernetics, UK). Real-time streaming is carried out using Debut software (NCH Software, USA).

An homogeneous particle solution is prepared with the use of full cell culture media (RPMI, Gibco, UK) with the addition of 5% bovine serum albumin (BSA) to make up to a similar viscosity. The concentration of the MDCP solution used here is 4×10^{10} per liter, a lower concentration than that used in the experiment of Avilés et al. [14]. There the concentration was 50 mg/liter which corresponds to 11.2×10^{10} per liter. These concentrations are calculated from the mass of one MDCP. In both concentrations the particles agglomerated and they create clusters. In this study, we use lower concentration of MDCP due to the higher magnetite load single MDCP containing 45.8 wt% magnetite whereas Avilés et al. [14] uses MDCP containing 25 wt% magnetite. To model the behavior of the MDCPs, we use smaller number of the MDCPs for lower concentration to match the experimental setup of Avilés et al. [14].

Once the MDT system is set up, control runs are carried out, with and without magnetic field to calibrate the system and monitor the particle trajectory and agglomeration in the absence of the stent.

The coil stent is then inserted into the tube and two homogeneous magnetic field strengths $\mu_0 H_0 = 0.15$ T and $\mu_0 H_0 = 0.60$ T are applied for different fluid velocities ranging between 0.58 cm/s and 52.6 cm/s. Once the magnetic field is applied the MDCPs were seen to agglomerate and create clusters. Different flow rates were chosen similar to those Avilés et al. [14]. For $\mu_0 H_0 = 0.15$ T magnetic field strength 0.05, 0.1, 0.2, 0.4, 1.0 cm/s injection velocities and for $\mu_0 H_0 = 0.60$ T magnetic field strength 0.2, 0.4, 1.0, 2.0, 4.5 cm/s injection velocities were used.

The amount of the MDCPs collected by the stent is measured by the differential between the MDCP concentration in the collection tube and the known initial particle concentration. Both solutions are measured by flow cytometry in triplicate counts.

After each particle solution injection the magnetic gradient was removed to demagnetize the superparamagnetic particles and to account for the mechani-

5

cally bound particle residuals (always $< 1\%$ of the overall injected volume).

3. Outline of Model

In order to effectively model this system, the 3D geometry of the stent and tube is reduced to 2D slice through the center of the tube (See Figure 2). Thus the coiled stent is modeled as a series of circular cross sections of an infinite wire with radius of R_{wire} located at the upper and lower boundaries of the walls. At each wall the wires are separated by a distance, h, between their centers, and the upper and lower sections are offset by $h/2$ as shown in Figure 2. It should be noted that physically this corresponds to a 2D description of flow with a parabolic profile in a rectangular box with transverse cylindrical wires, all of infinite extent. We model the behavior of N ($N < 25$) MDCPs under the influence of Stokes drag, a force due to hydrodynamic interaction, and a magnetic force, modified to incorporate the mutual magnetic dipole-dipole interaction. Other forces such as inertia and gravity are ignored. The Stokes drag for MDCP n is

$$\vec{F}_{\mathrm{s}_n} = 6\pi\,\eta_{\mathrm{f}}\,R_{\mathrm{p}_n}\,(\vec{v}_{\mathrm{f}} - \vec{v}_{\mathrm{p}_n}), \tag{1}$$

where η_{f} is the viscosity of the fluid, R_{p_n} is the radius of MDCP n, and $\vec{v}_{\mathrm{f}}$ and $\vec{v}_{\mathrm{p}_n}$ are the velocities of the fluid and MDCP n respectively. The fluid velocity, $\vec{v}_{\mathrm{f}}$, is determined by solving the appropriate Navier-Stokes equations. The motion of a MDCP through a viscous fluid creates a disturbance to the fluid flow, which will be felt by all other MDCPs. As a result, the other MDCPs experience a force which is said to result from hydrodynamic interaction with the original MDCP. By considering N MDCPs, the force due to the hydrodynamic interaction, $\vec{F}_{\mathrm{hyd}_n}$, which acts on MDCP n due to the presence of other $(N-1)$ MDCPs, can be written as,

$$\vec{F}_{\mathrm{hyd}_n} = \sum_{\substack{(i=1) \\ i \neq n}}^{N} \xi_{ni} \cdot \left(\vec{v}_{\mathrm{f}} - \vec{v}_{\mathrm{p}_i}\right) \tag{2}$$
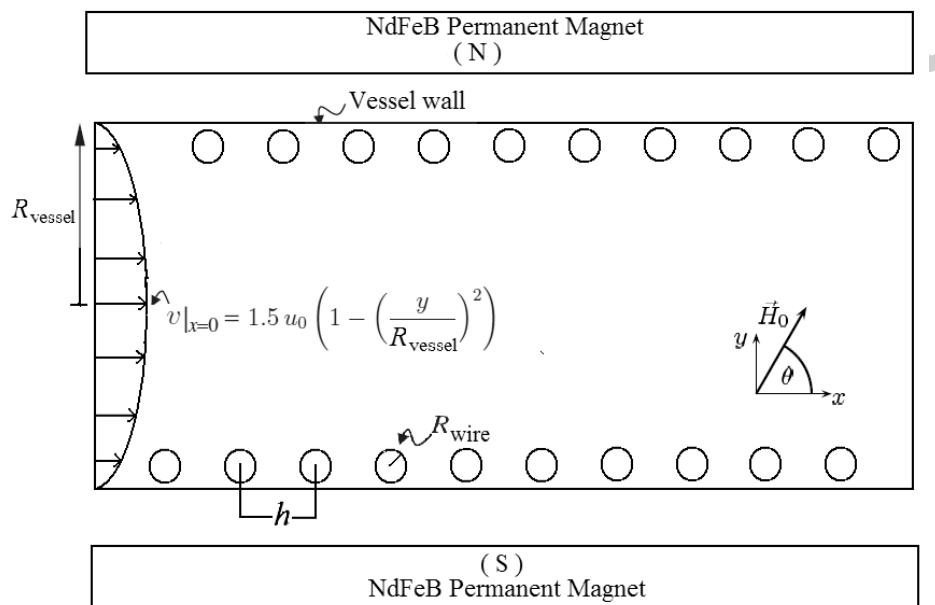
6

Figure 2: Schematic of the control volume (CV) used for determining the magnetizable stent collection efficiency (CE) through analysis of the corresponding MDCP trajectories. The CV has dimensions of $2\,\mathrm{cm}$ and $0.05\,\mathrm{cm}$ and encompasses a ten-loop stent within an expanded vessel. The MDCPs enter the CV from the left with a reduced average velocity defined by a parabolic profile and unexpanded average blood vessel velocity.

where ξ_{ni} is the modification due to the hydrodynamic interaction given by

$$\xi_{ni} = -6\pi \, \eta_{\mathrm{f}} \, R_{\mathrm{p}_n} \, \frac{3 \, R_{\mathrm{p}_i}}{4 \, |\vec{r}_n - \vec{r}_i|} \left(\mathbf{1} + \frac{(\vec{r}_n - \vec{r}_i) \otimes (\vec{r}_n - \vec{r}_i)}{|\vec{r}_n - \vec{r}_i|^2} \right) \tag{3}$$

where R_{p_i} is the radius of the MDCP i, $\mathbf{1}$ is the unit tensor, $\otimes$ is the vector tensor product (outer product), $\vec{r}_n$ and $\vec{r}_i$ are the positions of MDCP n and MDCP i, respectively. Initially all MDCPs are taken to have the same radius but after agglomeration, MDCPs of different radius are possible, as each agglomeration is viewed as a new MDCP of increased radius.

In general the magnetic force acting on a magnetic moment is determined by

$$\vec{F}_{\mathrm{m}} = (\vec{m} \cdot \nabla) \, \vec{B}_{\mathrm{total}}, \tag{4}$$

where $\vec{m}$ is the magnetic moment and $\vec{B}_{\mathrm{total}}$ is the total magnetic flux density. Magnetic dipoles exert a force on each other, which can be included in the magnetic force equation by considering (i) the modified magnetic flux density and (ii) the modification in the magnetic moment resulting from this modified flux density. With regard to the magnetic dipole-dipole interaction between N number of MDCPs, each MDCP is taken as spherical with radius R_{p_n} and sufficiently small to have homogeneous magnetic flux throughout the MDCPs. Hence, in order to include the magnetic effect on MDCP n of the other $(N-1)$ MDCPs, the modified magnetic force, $\vec{F}_{\mathrm{mm}_n}$, can be written as

$$\vec{F}_{\mathrm{mm}_n} = (\vec{m}_n \cdot \nabla) \, \vec{B}_{\mathrm{total}_n} \tag{5}$$

where $\vec{m}_n$ is the total magnetic moment of MDCP n, $\vec{B}_{\mathrm{total}_n}$ is the total magnetic flux acting on MDCP n. It can be taken as

$$\vec{B}_{\mathrm{total}_n} = \vec{B} + \sum_{\substack{(i=1) \\ (i \neq n)}}^{N} d\vec{B}_i \tag{6}$$

where $\vec{B}$ is the magnetic flux density due to the external field, $d\vec{B}_n$ is the modification of the resulting magnetic flux density due to MDCP n at $\vec{r}$. The

8

modification to the magnetic flux density is thus taken as

$$d\vec{B}_n(\vec{r}) = \frac{1}{3}\left(\mu_0\, M_{\text{fm,p,s}}\frac{L(\beta)}{B}\right)\,\frac{R_{\text{p}_n}^3}{|\vec{r}-\vec{r}_n|^3}\left(\frac{3\left(\vec{B}(\vec{r}_n)\cdot(\vec{r}-\vec{r}_n)\right)}{|\vec{r}-\vec{r}_n|^2}(\vec{r}-\vec{r}_n)-\vec{B}(\vec{r}_n)\right)$$

(7)

where μ_0 is the magnetic permeability of free space, $\vec{r}$ represents an arbitrary point in space, $\vec{B}(\vec{r}_n)$ is the flux density at $\vec{r}_n$ and $M_{\text{fm,p,s}}$ is the saturation magnetization of the ferromagnetic material in the MDCP. The value of $\vec{B}$ required to calculate the magnetic force as given by Eqs. (5) and (16), is calculated from the scalar magnetic potential due to the stent wires, which satisfies the Laplace equation over two con-joined regions: inside and outside the stent wires. Thus for outside the stent wires regions we have magnetic flux given by [9, 10, 11, 12, 13, 14, 15]

$$\vec{B} = \mu_0(\vec{H}_0 - \nabla\phi)$$

(8)

where $\vec{H}_0$ is the applied homogeneous magnetic field as in Figure 2 and ϕ represents the reduced magnetic scalar potential which in the region outside the stent wires is given by [20, 19, 21]

$$\phi = H_0\,R_{\text{wire}}^2\,\alpha_{\text{wire}}\,\frac{x\cos\theta + y\sin\theta}{x^2+y^2},$$

(9)

where R_{wire} is the radius of the stent wire implant, α_{wire} is the demagnetizing factor of the stent wire (given by Eq. (11)). The induced magnetization of the wire, $\vec{M}_{\text{wire}}$, is taken to be parallel to the external magnetic field, $\vec{H}_0$, and can be calculated from

$$\vec{M}_{\text{wire}} = 2\alpha_{\text{wire}}\vec{H}_0,$$

(10)

where α_{wire} is the demagnetizing factor for an infinitely long cylinder in a perpendicular field taken as

$$\alpha_{\text{wire}} = \min\left(\frac{\chi_{\text{wire},0}}{2+\chi_{\text{wire},0}}, \frac{M_{\text{wire,s}}}{2H_0}\right),$$

(11)

where $\chi_{\text{wire},0}$ and $M_{\text{wire,s}}$ are the zero field susceptibility and saturation magnetization of the ferromagnetic wire respectively and $\vec{H}_0$ can be written

$$\vec{H}_0 = \begin{pmatrix} H_0\cos\theta \\ H_0\sin\theta \end{pmatrix},$$

(12)

9

where H_0 is the magnitude of the applied field and θ is the direction of the applied magnetic field with respect to the x-axis, as in Figure 2.

It is assumed that the ferromagnetic material in each MDCP consists of smaller single domain spherical nanoparticles. Thus, the average projection of $\vec{m}$ the moment in the direction of $\vec{B}_{\text{total}}$ can be calculated from the Langevin function [6, 8, 22, 23, 24]

$$L\left(\beta\right) = \coth\left(\beta\right) - \frac{1}{\beta}, \tag{13}$$

with Langevin argument

$$\beta = \frac{m_{\text{fm,p}} B_{\text{total}}}{kT}, \tag{14}$$

where B_{total} is the magnitude of $\vec{B}_{\text{total}}$, k is Boltzmann's constant, T is the absolute temperature and $m_{\text{fm,p}}$ is the magnitude of the magnetic moment of the magnetite in the MDCPs. The magnetic moment of each magnetite nanoparticle within the MDCP, $\vec{m}_{\text{fm,p}}$, can be written as

$$\vec{m}_{\text{fm,p}} = V_{\text{fm,p}} M_{\text{fm,p,s}} \frac{\vec{B}}{B} \tag{15}$$

where $V_{\text{fm,p}}$ is the spherical volume of a single domain magnetite nanoparticle and $M_{\text{fm,p,s}}$ is the (volume) saturation magnetization of the magnetite inside the MDCPs. Note that $M_{\text{fm,p,s}}$ and $m_{\text{fm,p,s}}$ are fitting parameters in this model, obtained by Avilés *et al.* through characterization of the magnetic fluid [14].

Thus, the magnetic moment of the MDCP, $\vec{m}$, can be written as

$$\vec{m} = \omega_{\text{fm,p}} V_{\text{p}} M_{\text{fm,p,s}} L\left(\beta\right) \frac{\vec{B}}{B} \tag{16}$$

where V_{p} is the MDCP volume and $\omega_{\text{fm,p}}$ is the volume fraction of ferromagnetic material in the MDCP, related to its weight fraction $x_{\text{fm,p}}$ through [9]

$$\omega_{\text{fm,p}} = \frac{x_{\text{fm,p}}}{x_{\text{fm,p}} + (1 - x_{\text{fm,p}})\rho_{\text{fm,p}}/\rho_{\text{pol,p}}} \quad , \tag{17}$$

where $\rho_{\text{fm,p}}$ is the density of the ferromagnetic material in the MDCP and $\rho_{\text{pol,p}}$ is the density of the polymer material in the MDCP. In this model the value of $\omega_{\text{fm,p}}$ is measured through the experiment.

10

4. Fluid flow — the Navier-Stokes equations

The fluid is treated as an incompressible, Newtonian, isothermal, single-phase fluid with velocity $\vec{v}_f$ and pressure P at steady state flow. We have the continuity equation

$$\nabla \cdot \vec{v}_f = 0, \tag{18}$$

and the Navier-Stokes equation

$$\rho_f[(\vec{v}_f \cdot \nabla \vec{v}_f)] = \nabla P + \eta_f \nabla^2 \vec{v}_f, \tag{19}$$

where ρ_f is the density of the fluid. To solve Eqs. (18) and (19), a parabolic velocity profile is assumed at the inlet control volume (CV) such that

$$v_{f,x|x=0} = 1.5\, u_0 \left(1 - \left(\frac{y}{R_{\text{vessel}}}\right)^2\right), \tag{20}$$

$$v_{f,y|x=0} = 0 \tag{21}$$

where u_0 is the average inlet fluid velocity and R_{vessel} is the vessel (tube) radius. Furthermore, non-slip boundary conditions ($\vec{v}_f = 0$) are applied at the wire-fluid interface and at the upper and lower CV boundaries. Atmospheric pressure is assumed at the outlet of the CV to satisfy the boundary condition on pressure.

5. Velocity equations, Streamlines and Capture Cross Section

The velocity of a MDCP n can be obtained by summing the Stokes drag, the force due to hydrodynamic interaction and the modified magnetic force, as given in Eqs. (1), (2) and (5) respectively with inertial forces, $\vec{F}_{i_n}$, as

$$\vec{F}_{s_n} + \vec{F}_{\text{hyd}_n} + \vec{F}_{\text{mm}_n} = \vec{F}_{i_n}. \tag{22}$$

For MDCP n, by ignoring the inertial forces, $\vec{F}_{i_n}$, we rewrite Eq. (22) as

$$6\pi\, \eta_f\, R_{p_n} \left(\vec{v}_f - \vec{v}_{p_n}\right) + \sum_{\substack{(i=1) \\ i \neq n}}^{N} \xi_{ni} \cdot \left(\vec{v}_f - \vec{v}_{p_i}\right) + (\vec{m}_n \cdot \nabla)\left(\vec{B}_{\text{total}}\right)_n = 0. \tag{23}$$

Hence, we can obtain $\vec{v}_{p_n}$ by solving Eq. (23) numerically in each time step.

11

Finally, the trajectories of each MDCP can be obtained from evaluating the streamline functions [6,13]. The system performance of this mathematical model is calculated in terms of collection efficiency, CE, defined as

$$\text{CE} = \frac{2\,R_{\text{vessel}} - y_1 + y_2}{2\,R_{\text{vessel}}}\,100, \qquad (24)$$

where y_1 and y_2 are defined by the location of the streamline at the entrance to the CV of the last MDCPs captured by the stent wires (Figure 2). All calculations were performed using the open-source software finite volume library OpenFOAM [25].

6. Results and Discussions

In this paper, we include the effect of both magnetic dipole-dipole and hydrodynamic interactions for multiple MDCPs in the stent based mathematical model of Avilés *et al.* [14]. We focus on varying the initial positions of N ($N < 25$) MDCPs at the entrance of the CV and present the results in terms of the CE of the system considering the agglomeration of MDCPs.

Of interest is the effect of the velocity of the blood and the field strength on the CE of the system. This is shown in Figures 3–6 with both dipole-dipole magnetic and hydrodynamic interactions, experimental results and without any particle interactions.

In the 2D model, the behavior of the MDCPs after agglomeration is also considered. It is seen that the MDCPs create a cluster during their agglomeration as a result of both interactions. The volume of the cluster is calculated by summing the volume of the MDCPs agglomerated and the radius of the cluster is calculated using the general volume formulation ($4/3\,\pi\,r^3$) [26]. Whilst this assumption does not account fully for the resulting hydrodynamic volume, the effect of this assumption should not significantly affect our results.

6.1. Mathematical Model Explanation and Details

The rationale for the simulations is as follows. Given sufficient computing power, one might consider randomly distributing, particle in the form of a clus-

12

ter, a very large number ($> 10,000$) of MDCPs and allow interactions between all of these. With limited computing resources, one is forced to reduce this. We do this in two ways. Firstly, by limiting the regions of initial positions that we consider and secondly by limiting the number of MDCPs that we allow to mutually interact. Thus we consider only those parts of the simulation which are likely to contribute to any alteration in the CE. For instance, in those parts of the capture cross section closest to the vessel walls, one can expect no improvement in the CE. In fact it is only where the initial positions are close to the border between the collection and no collection region, that is around the boundary of the reference capture cross section that we start to see altered trajectories due to interactions. The boundary of the reference capture cross section (CCS), λ_c^* is the trajectory of the last MDCP, which would be captured by the stent wires in the non-interacting case. Secondly, the mutual interparticle interaction would not be expected to have infinite extent. One can postulate a number N^* of MDCPs in the model where the predicted difference in performance between modeling N^* and $N^* + 1$ becomes arbitrarily small. We point out that the computational effort required to model interactions scales with N^2, where N is the number of MDCPs interacting. Simulations were performed for increasing N, and the results indicate that there is no significant change to the system performance metrics beyond twenty five MDCPs.

In light of these factors, we consider a particular, homogeneously distributed cluster of N MDCPs. The MDCP concentration of the Avilés *et al.* system is 50 mg/l which corresponds to 11.2×10^{10} MDCPs per liter and the MDCP concentration of our experimental setup is 4×10^{10} per liter. The effective initial distance between the MDCPs in the CV is calculated using the concentration of the MDCPs in the glass tube. Initial distance is taken as the cube root of the MDCPs amount per liter $((dm)^3)$ and we created a homogeneous rectangular cluster of particles which mimic the experimental particle concentration flowing through the stent during the video streaming.

In order to describe the effect of both interactions we consider two different simulation configurations, similar to those used in a previous paper for the

13

inclusion of interactions between the two MDCPs and between the MDCPs and the fluid [19]. The first configuration is intended to illustrate the agglomeration of the MDCPs *within* the reference CCS region. In this configuration all of the MDCPs are captured, as expected and the resulting CE of the system for this situation is unaltered.

The second simulation configuration is intended to examine the effects of interactions on the CE of the system near the λ_c^*. For this, we place the center of the particle cluster on the λ_c^* for a given velocity and record changes in CE through following the MDCP trajectories in the normal way. We then shift the particle cluster up and down, and again record changes in CE. This approach is repeated for each increased fluid velocity, using, for a given field, the same particle cluster.

6.2. Comparison of the Mathematical Model Results and Literature

Initially, the results of our mathematical model and the experimental result of Avilés *et al.* are compared. Results are presented by calculating the CEs for identical MDCPs with initial radius $R_p = 0.435\,\mu\mathrm{m}$ containing $25\,\mathrm{wt\%}$ magnetite, under the influence of homogeneous magnetic field oriented perpendicularly to the flow ($\theta = \pi/2$) with magnitudes of $0.17\,\mathrm{T}$ to $0.65\,\mathrm{T}$. The glass tube radius size is taken as $0.05\,\mathrm{cm}$ as in the experiment of Avilés *et al.*. In the model the magnetization of the individual MDCPs is taken as the average value given by the Langevin function due to the single domain magnetic nanoparticles within. The relevant fluid flow properties and the properties of the ferromagnetic materials used in the MDCPs and for the stent wire, are given in Table 1.

For the configurations outlined above, we keep the applied field constant ($\mu_0 H_0 = 0.17$ T) and we increase the blood velocity from $u_0 = 2.1\,\mathrm{cm/s}$ to $u_0 = 42.4\,\mathrm{cm/s}$. The resulting CEs for these simulations are shown in Figure 3. Secondly, using the same methodology we applied $\mu_0 H_0 = 0.65$ T and vary the fluid velocity between $u_0 = 2.1\,\mathrm{cm/s}$ and $u_0 = 42.4\,\mathrm{cm/s}$. The resulting CEs are given in Figure 4.

14

Properties	Symbol	Units	Values	Data type
MDCPs Properties				
Polymer material	-	-	P(S/V-COOH)Mag	Physical
Radius	R_{p}	μm	0.435, **0.43**	Physical
Saturation magnetization	$M_{\mathrm{p,s}}$	kA/m	22.4	Measured
MDCPs Magnetic Material Properties				
Material	-	-	Magnetite	Physical
Weight content	$x_{\mathrm{fm,p}}$	wt%	25, **45.8**	Physical
Volume content	$\omega_{\mathrm{fm,p}}$	-	6.4	Measured
Saturation magnetization	$M_{\mathrm{fm,p,s}}$	kA/m	351.9	Measured
Magnetic moment	$m_{\mathrm{fm,p}}$	Am^2	2.03×10^{-19}	Measured
Radius	$R_{\mathrm{fm,p}}$	nm	5.18	Calculated
Physical Properties				
Number of Particles	-	particle/L	11.2×10^{10}, **4 $\times$ 10^{10}**	Physical
Temperature	T	K	300	Physical
Boltzmann's constant	k_B	J/K	1.38×10^{-23}	Physical
Permeability of vacuum	μ_0	Tm/A	$4\pi \times 10^{-7}$	Physical
Applied Field Properties				
Magnitude	$\mu_0 H_0$	T	0.0–0.7	Physical
Angle of field direction	θ	-	$\pi/2$	Physical
Stent Properties				
Material	-	-	SS 430	Physical
Wire radius	R_{wire}	μm	62.5	Physical
Loop separation	h	cm	0.2	Physical
Number of loops	N_l	-	10	Physical
Coil length	L	cm	2	Physical
Saturation magnetization	$M_{\mathrm{implant,s}}$	kA/m	1261	Measured
Magnetic susceptibility	$\chi_{\mathrm{implant,0}}$	-	1000	Physical
Blood & Vessel Properties				
Velocity	u_0	cm/s	2.1, 4.2, 10.6, 21.2, 42.4	Physical
	u_0	cm/s	**0.58, 1.17, 2.34, 4.68, 11.7, 23.4, 52.6**	Physical
Volume	V_{blood}	ml	10	Physical
Density	ρ_{b}	kg/m^3	1000	Physical
Viscosity	η_{b}	kg/ms	1.0×10^{-3}	Physical
Vessel radius	R_{vessel}	cm	0.05, **0.04**	Physical

Table 1: Experimental values of fluidic setup and material parameters used in the mathematical model of the stent based simulation. Bold values are used in our experiment. Some material parameters are in agreement with Avilés and coworker study [14].
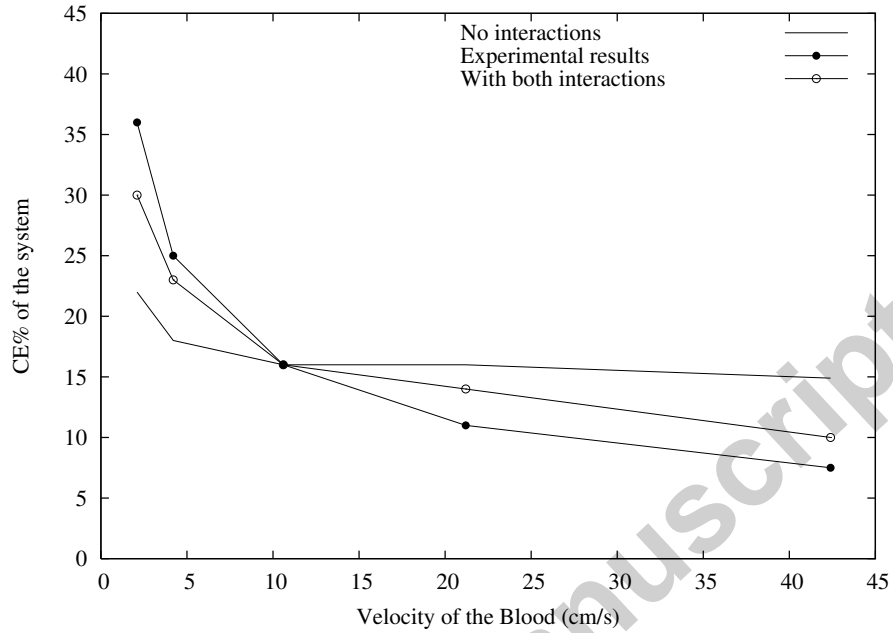
15

Figure 3: The collection efficiency (CE) of the system plotted as a function of the blood velocity $(2.1, 4.2, 10.6, 21.2, 42.4\,\text{cm/s})$ at the applied field $\mu_0 H_0 = 0.17$ T.

In Figures 3 and 4, the results of the mathematical model with the interactions show closer agreement with experimental results of Avilés *et al.* with low fluid velocity. This is due to the interaction and agglomeration of MDCPs in our model. With low fluid velocity ($\leq 10\,\text{cm/s}$) and higher applied field ($\mu_0 H_0 = 0.65$ T) MDCPs create a larger volume of cluster more easily than with the lower applied field ($\mu_0 H_0 = 0.17$ T). When we increase the fluid velocity the likelihood of the agglomeration of the MDCPs starts to decrease. For higher fluid velocity the CE of the IA-MDT system predicts lower collection than the results of Avilés model without interactions. This is due to the effect of hydrodynamic interactions on the velocity of MDCPs and so the trajectories of the MDCPs.

6.3. Comparison of the Mathematical Model and Experimental Results

Next, we compare the results of the mathematical model and *in vitro* experiments undertaken at CRANN TCD. Results are presented by calculating the
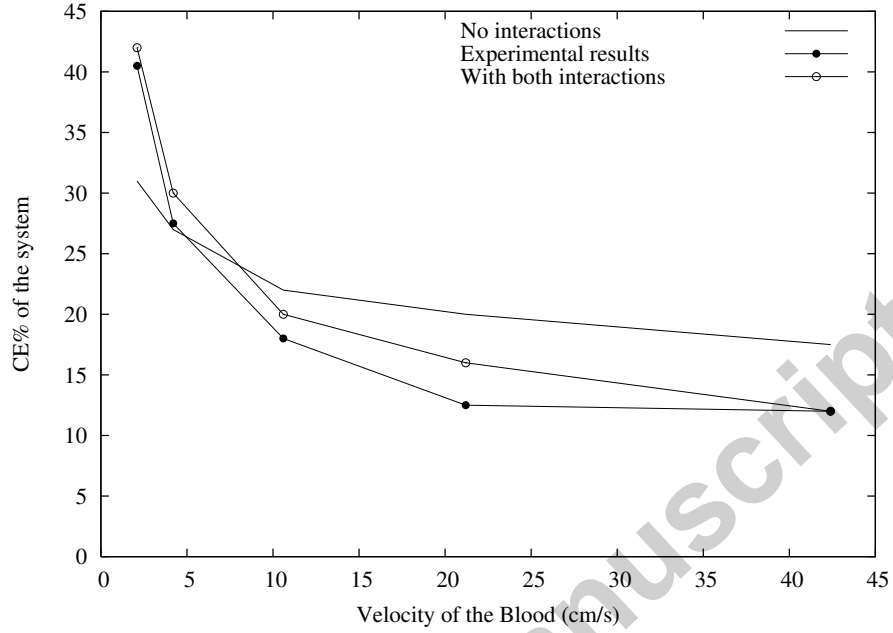
16

Figure 4: The collection efficiency (CE) of the system plotted as a function of the blood velocity $(2.1, 4.2, 10.6, 21.2, 42.4 \, \text{cm/s})$ at the applied field $\mu_0 H_0 = 0.65$ T.

CEs for identical MDCPs with initial radius $R_\text{p} = 0.43 \, \mu\text{m}$ containing $45.8 \, \text{wt}\%$ magnetite, under the influence of homogeneous magnetic field oriented perpendicularly to the flow $(\theta = \pi/2)$ with magnitudes of 0.15 T and 0.60 T. The glass tube radius size is 0.04 cm in our experiments. This was done to achieve a better image contrast between the particle layers aggregating on the stent during the experimental testing which is also increased by the smaller capillary diameter when compared to Avilés *et al.* [14] model.

In the model the magnetization of the individual MDCPs is taken as the average value given by the Langevin function due to the single domain magnetic nanoparticles within. The relevant fluid flow properties and the properties of the ferromagnetic material used in the MDCP and for the stent wire, are given in Table 1.

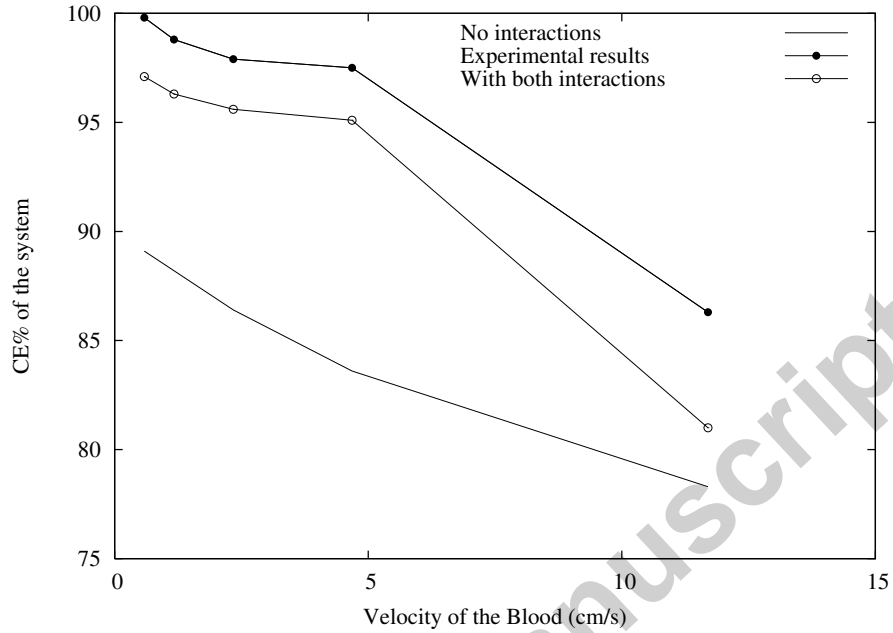For the configurations outlined above, we keep the applied field constant

17

Figure 5: The collection efficiency (CE) of the system plotted as a function of the blood velocity $(0.58, 1.17, 2.34, 4.68, 11.7 \, \mathrm{cm/s})$ at the applied field $\mu_0 H_0 = 0.15$ T.

$(\mu_0 H_0 = 0.15$ T) and we increase the blood velocity up to $u_0 = 11.7 \, \mathrm{cm/s}$. The resulting CEs for these simulations are shown in Figure 5. Secondly, we apply $\mu_0 H_0 = 0.60$ T and increase the fluid velocity up to $u_0 = 52.6 \, \mathrm{cm/s}$. The resulting CEs are given in Figure 6. In Figures 5 and 6, the results of the model with the interactions show closer agreement with the measured experimental results. The results shown also highlight how a 0.01 cm reduction in the capillary radius can affect the collection efficiency. This leads to speculation over a higher efficacy of the MDCT technique at the level of peripheral circulatory capillary vessels. On the other hand, this increased CE efficiency also increases the risk of vessels clotting and thrombolytic effect especially when also accounting for the presence of the solid part of the blood [27].

Collection Efficiency is a key parameter for the modeling validation of the experimental testing. Differences between Avilés *et al.* and our experimental
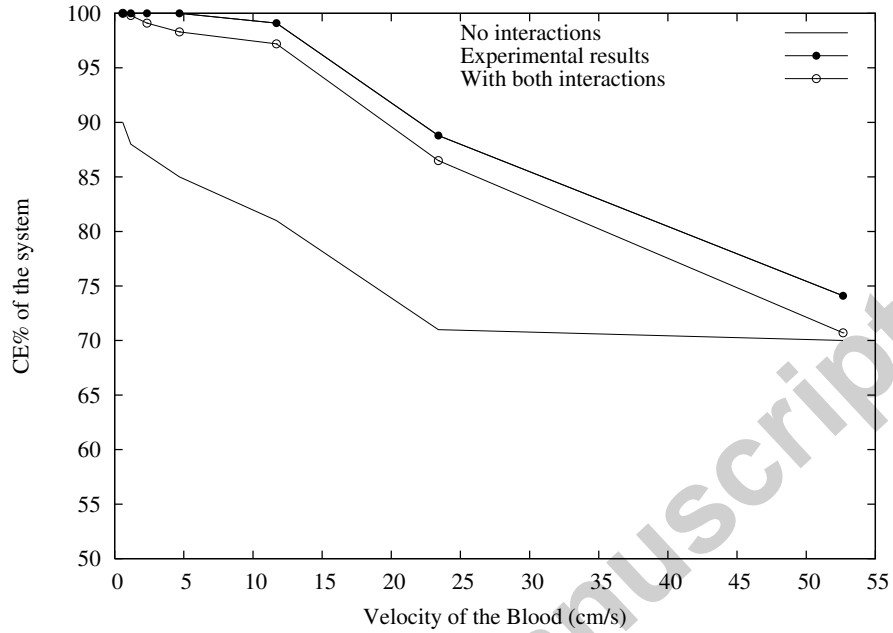
Figure 6: The collection efficiency (CE) of the system plotted as a function of the blood velocity $(2.34, 4.68, 11.7, 23.4, 52.6\,\mathrm{cm/s})$ at the applied field $\mu_0 H_0 = 0.60$ T.

model (Cregg *et al.*) are shown in Table 2.

7. Conclusions

We have presented an interaction model applied to IA-MTD. This model considered the agglomeration of particles known to occur in such systems [12, 14, 15]. We include the effects of both the dipole-dipole and hydrodynamic interactions for multiple particles in stent implant arrangements. The resulting collection efficiencies derived from the mathematical model are in closer agreement with our latest experimental results and those presented by Avilés *et al.*. Furthermore, the mathematical model presented in this work represents a useful analytical tool for the prediction of the efficacy of targeted drug delivery by superparamagnetic particles. The implications in the nanotechnology and nanomedicine research area are based on the efficiency in delivering the drug

19

Parameters	Avilés *et al.* model	Cregg *et al.* model
Vessel radius (cm)	0.05	0.04
Velocity Range (cm/s)	2.1–42.4	0.58–52.6
Magnetic Field (T)	0.17, 0.65	0.15, 0.60
Number of Repeats	-	10

Table 2: Differences between Avilés *et al.* and Cregg *et al.* experimental model.

coated particles within the magnetizable stent length.

8. Acknowledgements

References

[1] W. P. Torchilin, Drug targeting, J. Pharm. Sci. 11 (2000) S81–S91.

[2] D. J. A. Crommelin, G. Scherphof, G. Storm, Active targeting with particulate carrier systems in the blood compartment, Adv. Drug Deliv. Rev. 17 (1995) 49–60.

[3] A. S. Lübbe, C. Bergemann, J. Brock, D. G. McClure, Physiological aspects in magnetic drug-targeting, J. Magn. Magn. Mater. 194 (1999) 149–155.

[4] A. S. Lübbe, C. Aleciou, C. Bergemann, Clinical applications of magnetic drug targeting, J. Surg. Res. 95 (2001) 200–206.

[5] A. J. Lemke, M.-I. S. von Pilsach, A. S. Lübbe, C. Bergemann, H. Riess, R. Felix, MRI after magnetic drug targeting in patients with advanced solid malignant tumors., Eur. Radiol. 14 (2004) 1949–1955.

[6] A. D. Grief, G. Richardson, Mathematical modelling of magnetically targeted drug delivery, J. Magn. Magn. Mater. 293 (2005) 455–463.

[7] G. Iacob, O. Rotariu, N. J. C. Strachan, U. O. Häfeli, Magnetizable needles and wires - modeling an efficient way to target magnetic microspheres in vivo, Biorheology 41 (2004) 599–612.

[8] B. B. Yellen, Z. G. Forbes, D. S. Halverson, G. Fridman, K. A. Barbee, M. Chorny, R. Levy, G. Friedman, Targeted drug delivery to magnetic implants for therapeutic applications, J. Magn. Magn. Mater. 293 (2005) 647–654.

[9] J. A. Ritter, A. D. Ebner, K. D. Daniel, K. L. Stewart, Application of high gradient magnetic separation principles to magnetic drug targeting, J. Magn. Magn. Mater. 280 (2004) 184–201.

[10] H. Chen, A. D. Ebner, M. D. Kaminski, A. J. Rosengart, J. A. Ritter, Analysis of magnetic drug carrier particle capture by a magnetizable intravascular stent: Parametric study with multi-wire two-dimensional model, J. Magn. Magn. Mater. 293 (2005) 616–632.

[11] A. J. Rosengart, M. D. Kaminski, H. Chen, P. L. Caviness, A. D. Ebner, J. A. Ritter, Magnetizable implants and functionalised magnetic carriers: A novel approach for non-invasive yet targeted drug delivery, J. Magn. Magn. Mater. 293 (2005) 633–638.

[12] M. O. Avilés, A. D. Ebner, H. Chen, A. J. Rosengart, M. D. Kaminski, J. A. Ritter, Theoretical analysis of a transdermal ferromagnetic implant for retention of magnetic drug carrier particles, J. Magn. Magn. Mater. 293 (2005) 605–615.

[13] M. O. Avilés, A. D. Ebner, J. A. Ritter, Ferromagnetic seeding for the magnetic targeting of drugs and radiation in capillary beds, J. Magn. Magn. Mater. 310 (2007) 131–144.

[14] M. O. Avilés, A. D. Ebner, J. A. Ritter, Implant assisted-magnetic drug targeting: Comparison of in vitro experiments with theory, J. Magn. Magn. Mater. 320 (2008) 2704–2713.

[15] M. O. Avilés, A. D. Ebner, J. A. Ritter, In vitro study of magnetic particle seeding for implant assisted-magnetic drug targeting, J. Magn. Magn. Mater. 320 (2008) 2640–2646.

[16] M. O. Avilés, A. D. Ebner, J. O. Mangual, J. A. Ritter, Isolated swine heart ventricle perfusion model for implanted assited-magnetic drug targeting, Int. J. Pharm. 361 (2008) 202–208.

[17] H. B. C. I. Mikkelsen, M. F. Hansen, Theoretical comparison of magnetic and hydrodynamic interactions between magnetically tagged particles in microfluidic systems, J. Magn. Magn. Mater. 293 (2005) 578–583.

[18] R. Mehasni, M. Feliachi, M. Latreche, Effect of the magnetic dipole-dipole interaction on the capture efficiency in open gradient magnetic seperation, IEEE Trans. Magn. 43 (2007) 3488.

[19] P. J. Cregg, K. Murphy, A. Mardinoglu, Inclusion of magnetic dipole-dipole and hydrodynamic interactions in implant assisted magnetic drug targeting, J. Magn. Magn. Mater. 321 (2009) 3893–3898.

[20] P. J. Cregg, K. Murphy, A. Mardinoglu, Calculation of nanoparticle capture efficiency in magnetic drug targeting, J. Magn. Magn. Mater. 320 (2008) 3272–3275.

[21] K. J. Binns, P. J. Lawrenson, C. W. Trowbridge, The analytical and numerical solution of electric and magnetic Fields, Wiley, 1992, sec 3.2.2.

[22] P. J. Cregg, L. Bessais, Series expansions for the magnetisation of a solid superparamagnetic system of non-interacting particles with anisotropy, J. Magn. Magn. Mater. 202 (1999) 554–564.

[23] M. I. Shliomis, Magnetic fluids, Sov. Phys. Usp. 17 (1974) 153–169.

[24] H. C. Bryant, D. A. Sergatskov, D. Lovato, N. L. Adolphi, R. S. Larson, E. R. Flynn, Magnetic needles and superparamagnetic cells, Phys. Med. Biol. 52 (2007) 4009–4025.

[25] OpenCFD Ltd, OpenFOAM 1.4, http://www.opencfd.co.uk (2007).

[26] E. Allen, P. Smith, J. Henshaw, A review of particles agglomeration, US Department of Energy.

[27] W. Dzwinel, K. Boryczko, D. A. Yuen, A discrete-particle model of blood dynamics in capillary vessels, Journal of Colloid and Interface Science 258 (2003) 163–173.